Advanced Composites and Hybrid Materials (2024) 7:111
https://doi.org/10.1007/s42114-024-00926-2

RESEARCH

Enhanced biogas upgrading by photocatalytic conversion of carbon dioxide to methane by *Methanosarcina barkeri*–cadmium sulfide biohybrid

Ziyu Wang[1] · Mingyu Gou[2] · Qiyuan Zheng[1] · Haiyu Xu[3] · Saad Melhi[4] · Zeinhom M. El-Bahy[5] · Eman Ramadan Elsharkawy[6] · Yan Dang[1] · Bin Qiu[1]

Received: 29 February 2024 / Revised: 16 June 2024 / Accepted: 19 June 2024 / Published online: 27 June 2024

Abstract
The semiconductive cadmium sulfide (CdS) nanoparticles were coated on the surface of *Methanosarcina barkeri* (*M. barkeri*) by self-assembly method to form the *M. barkeri*-CdS biohybrid in this work. It proved to be an effective and selective catalyst for the solar-driven conversion of CO_2 to CH_4, enabling the upgrading of biogas from anaerobic digestion. The physicochemical properties of the synthesized biohybrid were characterized, and the effect of various conditions on the CH_4 production of the biohybrid was also investigated. It was revealed that the CdS dosage, pH, cysteine, and concentration of sodium bicarbonate were key factors influencing the performance of the biohybrid. Additionally, it was observed that CH_4 was produced under both light and dark conditions. Finally, the mechanisms involved in the CH_4 production by the biohybrid under light and dark conditions were discussed.

Keywords Biohybrid · Methanogenesis · CO_2 conversion

1 Introduction

Transforming organic pollutants into biogas by anaerobic digestion is an effective method for recovering renewable energy from wastewater [1, 2]. CH_4 with a high calorific value is the main content in the biogas [3, 4]. However, more than 30% of CO_2 is typically present in biogas, reducing its energy density and confining its further applications [5, 6]. The conversion of CO_2 into valuable products such as biodiesel, bioethanol, or additional biogas has aroused wide concern with a view to diminish carbon footprint [7–10]. Among the various approaches, a feasible strategy to comply with the specifications of natural gas pipelines is the promotion of CO_2 biomethanation and biogas upgrading [11–15].

Various methods have been applied to purify and upgrade biogas from anaerobic digestion, including membrane separation [16], cryogenic separation [17], pressure swing adsorption [18], water scrubbing [19], physical scrubbing, chemical adsorption [20], and biological conversion [6]. Bio-electrochemical systems (BES) are recognized as an effective biological conversion method, gaining attention for their capability to increase the CH_4 content in biogas up to 98% [21]. The semi-artificial photosynthetic biohybrid, composed of semiconductors and archaea, is considered as another environmentally friendly biological conversion method [22]. The biohybrid integrates the light-harvesting capability of semiconductors with the replicative abilities of microorganisms to fulfill photocatalytic objectives, thereby enhancing solar power conversion efficiency in comparison

Ziyu Wang and Mingyu Gou contributed equally.

✉ Bin Qiu
qiubin2015@bjfu.edu.cn

[1] Beijing Key Laboratory for Source Control Technology of Water Pollution, College of Environment Science and Engineering, Beijing Forestry University, Beijing 100083, China

[2] Paris Elite Institute of Technology, Shanghai Jiao Tong University, Shanghai 200240, China

[3] Qinglin Chuangneng (Shanghai) Technology Co., Ltd, Shanghai 201800, China

[4] Department of Chemistry, College of Science, University of Bisha, 61922 Bisha, Saudi Arabia

[5] Department of Chemistry, Faculty of Science, Al-Azhar University, Nasr City 11884, Cairo, Egypt

[6] Department of Chemistry, Faculty of Science, Northern Border University, Arar, Saudi Arabia

to conventional photosynthesis in plants [23–25]. Carbonate solutions were employed to selectively absorb CO_2 components in biogas, and the biohybrid subsequently converted the separated CO_2 into CH_4. Under illuminated environments, semiconductors capture photons directly on their surface, generating electron–hole pairs [26, 27]. These pairs undergo spatial separation facilitated by sacrificial reagents, releasing electrons and forming reduction equivalents [28]. By establishing appropriate connections between membrane-bound cytochrome proteins and semiconductors, archaea can specifically utilize the electrons to reduce CO_2 to CH_4 [29].

Recently, *Methanosarcina Barkeri*–cadmium sulfide (*M. barkeri*-CdS) biohybrid has been successfully synthesized and demonstrated to be effective in converting CO_2 to CH_4 with a yield of 0.19 μmol/h [30]. In order to improve the CH_4 production efficiency, Ni was further doped on the CdS, forming the *M. barkeri*-Ni: CdS biohybrid and the CH_4 yield was increased by ~ 2.5 times compared to the *M. barkeri*-CdS biohybrid [31]. To minimize the production of H_2 as a common by-product, Ni and Cu were integrated at the interface between the CdS and *M. barkeri*, and the obtained *M. barkeri*-NiCu@CdS biohybrid demonstrated a CH_4 selectivity of 100% and a quantum yield of 12.41 ± 0.16% [32]. To address the efficiency mismatch between electron production and utilization in *M. barkeri*-CdS biohybrid, a metal-free polymer carbonitride (CNx) modified with a unique capacitor cyanamide (NCN) group was used as the semiconductor to form the *M. barkeri* -^{NCN}CNx biohybrid and the CH_4 selectivity achieved 92.30% in this biohybrid [33]. An *M. barkeri*–carbon dot-functionalized polymeric carbon nitrides (CDPCN) photocatalytic system was developed by assembling *M. barkeri* and CDPCN, achieving a CH_4 selectivity of nearly 100% with the assistance of CO_2 [34]. Besides, an *R. palustris*/CdS biohybrid was also found to effectively convert CO_2 to CH_4 [35].

For upgrading biogas from the anaerobic wastewater treatment, *M. barkeri* has been identified as a suitable microorganism for biohybrid due to its obligate production of CH_4, high tolerance of adverse environments, and extracellular electron transfer ability [36, 37]. CdS, owing to the advantages of modifiable band gaps (Eg ~ 2.4 eV), multiple binding sites, good biocompatibility, and effective light capture, is an appropriate semiconductor for the biohybrid [38–42]. *M. barkeri*-CdS biohybrid has been demonstrated to effectively convert CO_2 to CH_4; thus, it is supposed to be a proper biohybrid for biogas upgrading. However, the effect of the key factors such as CdS dosage, pH, cystine, and sodium bicarbonate concentration on the conversion efficiency of the biohybrid still needs to be further investigated to obtain the optimal conditions for biogas upgrading.

In this work, a biohybrid was constructed using the CdS and *M. barkeri* as semiconductors and electroactive methanogens, respectively. The *M. barkeri*-CdS biohybrid was characterized, and the effect of CdS dosage in the biohybrid, pH, cystine, and sodium bicarbonate concentration on the transformation efficiency was investigated. Finally, the elemental composition and photochemical properties of the biohybrid with and without light were investigated to understand the mechanism of converting CO_2 to CH_4 by the *M. barkeri*-CdS biohybrid.

2 Materials and methods

2.1 Synthesis of *M. barkeri*-CdS biohybrid

Firstly, *M. barkeri* was incubated in the medium (Supplementary Table S1) in the serum bottle at 37 °C in a constant temperature incubator (FCE-3000, Kuntian, Shanghai, China) until it reached the late exponential phase. The culture was subsequently transferred into 50 mL of fresh substrate medium at a ratio of 1:5 for the secondary cultivation for 1–2 days. Once the OD_{600} of the culture reached 0.2 [43], 10 mL of the solution was added to a 20-mL anaerobic tube with $CdCl_2$ solution and then incubated for an additional 2–3 days. The culture was conducted in a constant temperature shaker (SHZ-82, LICHEN, Shanghai, China) in darkness. The speed was maintained at 120 rpm/min, and the temperature was controlled at 37 ℃. When the color of the solution changed to bright yellow, the solid was separated from the culture, obtaining the *M. barkeri*-CdS biohybrid.

2.2 Characterizations of the biohybrid

The morphology of the biohybrid was characterized using a scanning electron microscope (SEM 500, Zeiss, Germany) [44], whereas the elemental composition was determined through energy dispersive spectroscopy (EDS; AMETEK, Octane elect super, USA). The biohybrid was immobilized with glutaraldehyde and underwent gradient elution with ethanol before the detection. Further microstructural insights were obtained using field emission transmission electron microscopy (FETEM, Tecnai G2 F30, FEI, America) following the previous method [45]. The functional groups of the biohybrid were analyzed by Fourier transform infrared spectrometry (FTIR; Vertex 70, Bruker, Germany), and sample preparation followed the established protocols in the literature [46]. The valence of elements in the biohybrids was determined by using X-ray photoelectron spectroscopy (XPS, 250XI, Escalab, Britain) [47]. The optical properties of the biohybrid were evaluated through ultraviolet–visible (UV–vis) spectroscopy to determine the absorbance at different wavelengths via the coefficient spectrum test. The band gap (Eg) of the biohybrid was calculated following the method in the literature [48]. Photocurrent (*I-t*) and

electrochemical impedance spectroscopy (EIS) were conducted using a CHI620E electrochemical workstation (Chenhua, Shanghai, China). A glass carbon, platinum sheet, and silver chloride were used as anode, cathode, and reference electrode, respectively. A polarization potential of − 0.4 V was applied using a constant potential polarization mode.

2.3 CH_4 production by the biohybrid

The medium without organic substrates was aerated and sterilized for further use in the experiments (Supplementary Table S1). For each trial, 10 mL of the synthesized biohybrid was added to a 50-mL medium in an anaerobic serum bottle. The bottle was sealed and injected with 40 mL of mixed gas consisting of 20% CO_2 and 80% N_2 [49]. Then, the mixture was incubated in an incubator maintained at 37 ℃. A 25-W LED light functioned as a solar energy simulator. The biogas generated was collected by extracting 1 mL of biogas from the serum bottles using a syringe. To maintain internal pressure, 1 mL of mixed gas (20% CO_2 and 80% N_2) was then injected into the bottle. The gas chromatograph (GC7900, Yunneng International Scientific Instruments, Beijing, China) was used to analyze the CH_4 content in the biogas [50], with nitrogen serving as the carrier gas at a pressure of 0.4 MPa. The temperatures of the column oven, injector, and thermal conductivity detector were maintained at 120 °C, 140 °C, and 150 °C, respectively.

3 Results and discussion

3.1 Characterization of the biohybrid

SEM images showed the spherical morphology of the *M. barkeri*-CdS biohybrid with a rough surface, and the particles were attached to the surface of the *M. barkeri* (Fig. 1a). TEM images further illustrated that the CdS particles were uniformly distributed on the surface of the *M. barkeri* (Fig. 1b). EDS mapping showed a similar distribution of sulfur (S) and cadmium (Cd) elements (Fig. 1c,d). The uniformly distributed S and Cd elements as well as the well-dispersed carbon (C) and oxygen (O) elements confirmed the successful synthesis of CdS particles on the surface of *M. barkeri* (Supplementary Fig. S1), indicating the formation of *M. barkeri*-CdS biohybrid.

XPS analysis confirmed the presence of the S, C, Cd, and O elements in the biohybrid (Supplementary Fig. S2). The Cd 3d XPS spectrum showed the peaks located at 404.9 eV and 411.5 eV, which corresponded to Cd 3d5/2 and 3d3/2 (Fig. 1e). This indicated Cd in the biohybrid existed in the form of Cd^{2+} state [51, 52]. The S 2p3/2 peaks at 161 eV and 161.3 eV were attributed to S^{2-} (Fig. 1f), whereas the peak at 164 eV indicated elemental sulfur (S^0) [53], with the predominance of S^{2-} peaks in the spectra. These results verified the adhesion of CdS on the surface of *M. barkeri*, confirming the successful formation of

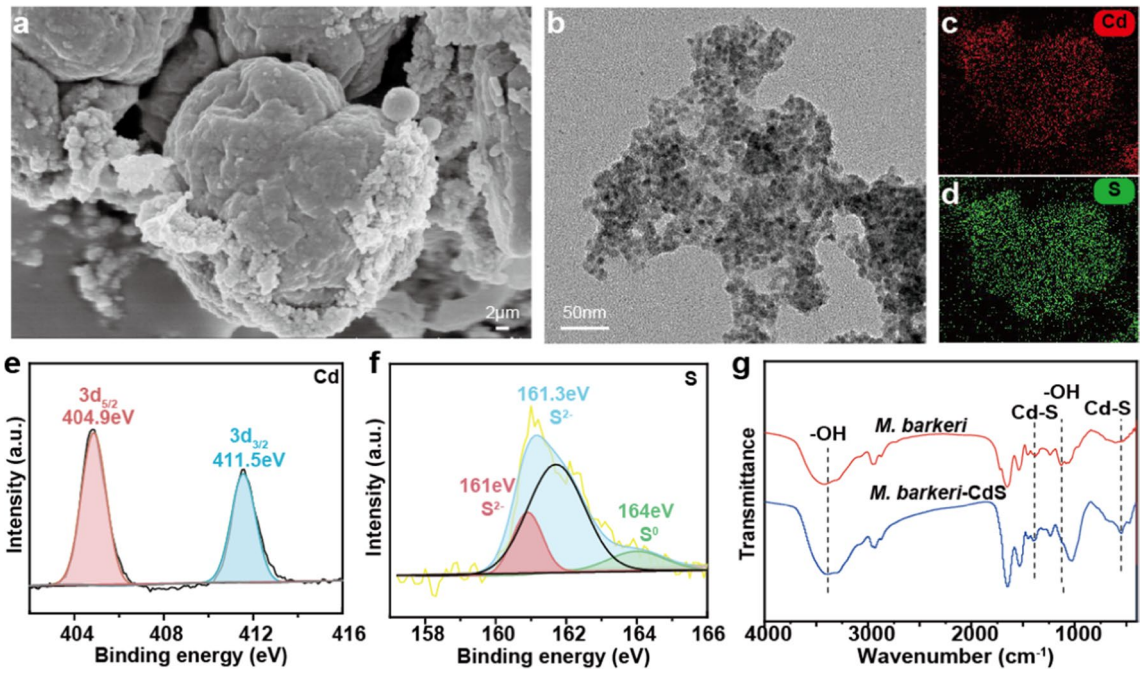

Fig. 1 (**a**) SEM image and (**b**) TEM image of the synthesized biohybrid. EDS mapping of (**c**) Cd and (**d**) S elements in the biohybrid. (**e**) Cd 3d and (**f**) S 2p XPS, and (**g**) FTIR spectra of the biohybrid

the *M. barkeri*-CdS biohybrid. The stability of intrinsic functional groups within the biohybrid was evaluated by FT-IR (Fig. 1g). Characteristic peaks at 550 cm^{-1} and 1399 cm^{-1} for Cd-S tensile vibrations, along with high-intensity peaks at 1028 cm^{-1} and 3389 cm^{-1} for hydroxyl group vibrations were observed [45]. Notably, the hydroxyl peak at 1028 cm^{-1} showed a red shift in the biohybrid, indicating the interaction between the CdS and *M. barkeri* in the biohybrid. The groups play a pivotal role in inhibiting hole-electron recombination and enhancing active site exposure [54], thereby facilitating electron transfer in the CH_4 production process.

3.2 Methane production by the biohybrid

CdS particles act as the semiconductor for the electron generation in the biohybrid, which plays a vital role in CH_4 production. $CdCl_2$ was used as the percussor for CdS; thus, its concentration affects CdS formation in the biohybrid, and excessive Cd^{2+} inhibits methanogenesis [55]. The effect of $CdCl_2$ addition for the biohybrid on the conversion of CO_2 to CH_4 under light exposure was investigated (Fig. 2a). Initially, 0.094-mL CH_4 was generated from the system added with pure *M. barkeri*, which was mainly attributed to residual organic matters in the system. When the $CdCl_2$ dosage was 0.5 mM (maintaining a 1:1 $CdCl_2$:Na_2S molar ratio), the maximum CH_4 production rate reached 65.42 μL/h on the first day, and the cumulative CH_4 yield was 1.76 mL. Then, the CH_4 production decreased with the increase in $CdCl_2$ dosage. The addition of 0.75-mM $CdCl_2$ initially slowed down CH_4 production, but on the fourth day, the CH_4 yield reached 37.72 μL/h. When $CdCl_2$ dosage was increased to 1 mM ($CdCl_2$:Na_2S ratio of 2:1), CH_4 production was significantly reduced to 0.043 mL. This is consistent with the results reported in the previous literature [30, 56]. A high concentration of Cd^{2+} stimulated the release of reactive oxygen species and suppressed the activity of *M. barkeri*, inhibiting CO_2 reduction to CH_4. Thus, the optimal $CdCl_2$ dosage for the biohybrid was recommended to be 0.5 ~ 0.75 mM.

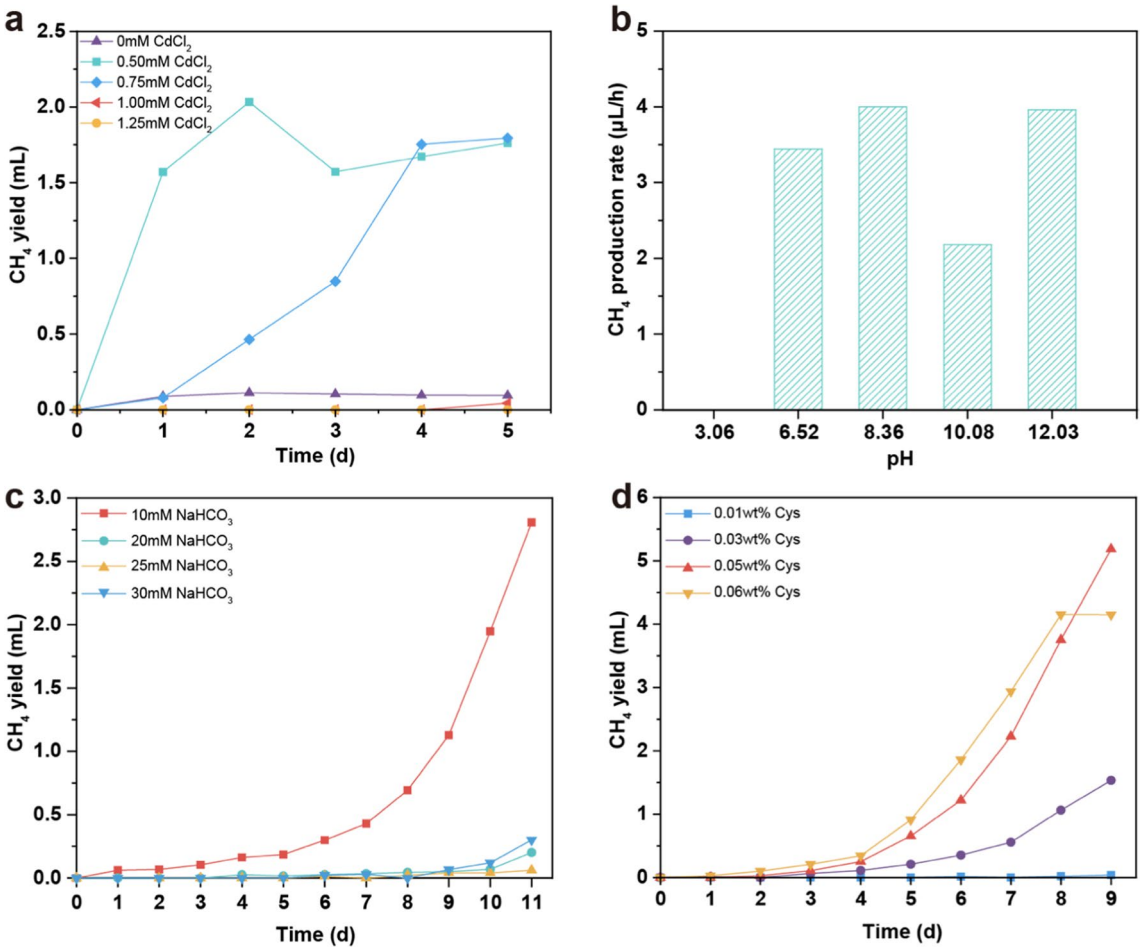

Fig. 2 Effect of (**a**) concentrations of $CdCl_2$, (**b**) pH values, and (**c**) concentrations of $NaHCO_3$ and (**d**) Cys on the methanation performance of the synthesized biohybrid

Bicarbonate solution was used as a carbon source for CO_2 reduction by the *M. barkeri*-CdS biohybrid [57]. pH value of the solution determines the forms of the carbon, which significantly influences the metabolic processes of *M. barkeri* [58]. The effect of the pH of the bicarbonate solution on CH_4 production by the *M. barkeri*-CdS biohybrid was investigated. As shown in Fig. 2b, CH_4 generation was minimal at a pH below 3.5 due to the highly acidic conditions inhibiting the growth, metabolism, and acid–base balance of *M. barkeri* in the biohybrid. Moreover, 3.44 mL, 4.00 mL, 2.18 mL, and 3.96 mL CH_4 were produced from the systems at pH levels of 6.52, 8.36, 10.08, and 12.03, respectively. The highest CH_4 production rate of 0.5 mL/h was detected at pH 8.36, and no obvious decrease was observed when the pH of the system changed. As was known, H_2CO_3 and HCO_3^-, the main forms of carbon existing in the solution under the acidic condition, are challenging to use by the *M. barkeri* in the biohybrid, which leads to a low CH_4 production rate. CO_2 and CO_3^{2-} are the main forms of carbon when the pH of the reaction system is neutral and alkaline. The CO_2 is readily available for utilization by the *M. barkeri*, and the *M. barkeri* is more active under neutral conditions [59], which resulted in a high CH_4 production rate. However, the CH_4 production rate remained high when the pH was increased to 12.03, which indicated that the *M. barkeri* in the biohybrid displayed strong resistance to alkaline solution. This is important for the utilization of biohybrid in biogas upgrading.

Bicarbonate acts as a CO_2 source for CH_4 production and buffer solution in the system [33, 60]. The effect of bicarbonate concentration on the CH_4 production by *M. barkeri*-CdS biohybrid was investigated (Fig. 2c); 2.81 mL of CH_4 was detected in the system with 10 mM of bicarbonate, and the CH_4 production decreased obviously with increasing bicarbonate concentration in the solution. This indicates that increased bicarbonate levels can negatively affect CH_4 generation, possibly due to the toxicity of Na^+ on the activity of *M. barkeri* in the biohybrid [61, 62]. Cysteine (Cys) has a dual role as a sulfur source for CdS synthesis and a reducing agent for capturing the generated holes in the biohybrid [63]. The effect of Cys dosage on CH_4 production by the biohybrid was evaluated (Fig. 2d). High CH_4 production was detected when the Cys dosage was 0.05 wt%, and it had a slight decrease when the Cys dosage increased; 4.15 mL of CH_4 was produced when 0.06 wt% of Cys was added into the reaction system. The added Cys captured the holes generated from the CdS under illumination, which avoids the damage of *M. barkeri* by the oxidative intermediates. It can also promote electron–hole separation, facilitating photoelectron utilization and CO_2 reduction by *M. barkeri* [64, 65].

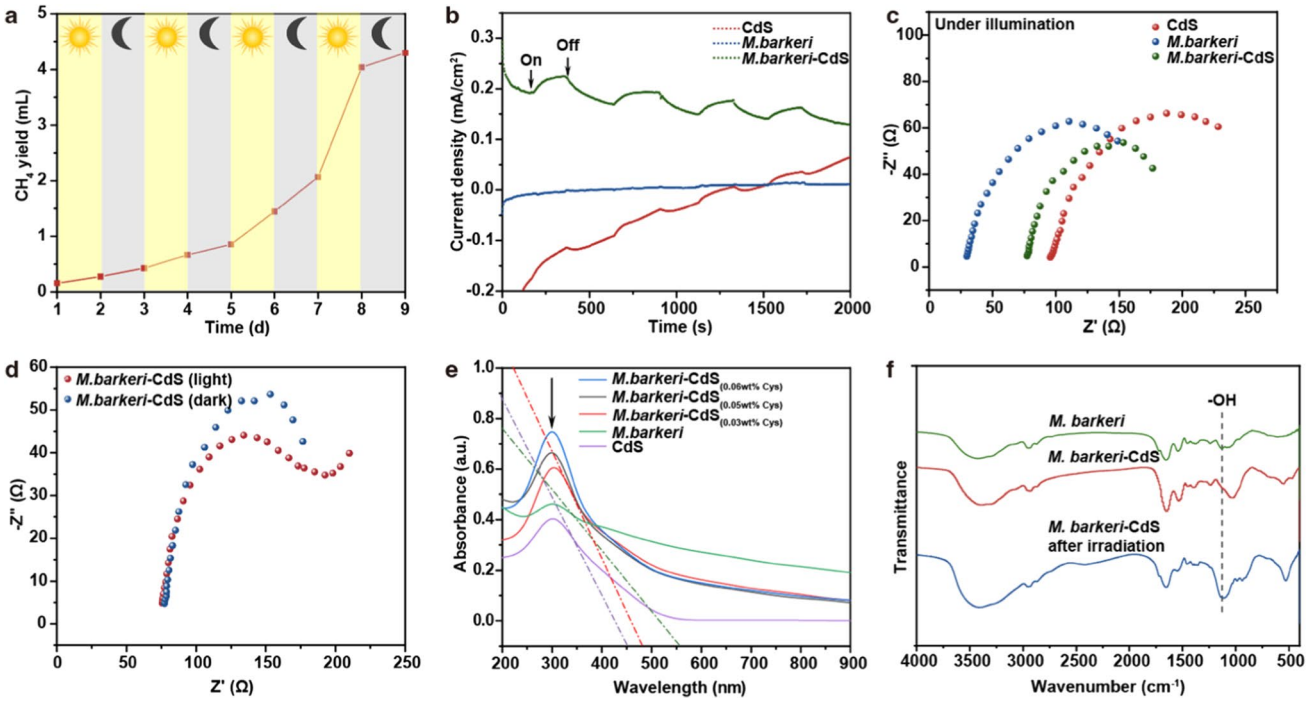

Fig. 3 (**a**) CH_4 yields of the synthesized biohybrid; (**b**) the *I*-t curve of pure *M. barkeri*, CdS, and biohybrid during light on/off cycles; (**c**) Nyquist plots of pure *M. barkeri*, CdS, and biohybrid under illumination; (**d**) Nyquist plots of the biohybrid under illumination and dark; (**e**) UV–Vis absorption spectra of pure *M. barkeri*, CdS, and biohybrid with different concentrations of Cys; (**f**) FT-IR of the pure *M. barkeri* and biohybrid before and after illumination

3.3 Electron transfer in the biohybrid

CH_4 production by the biohybrid was detected through the light–dark cycle, each consisting of 24 h of light followed by 24 h of darkness. There was a significant increase in CH_4 production, with a total yield of 4.30 mL after four cycles of incubation (Fig. 3a). It was revealed that CH_4 can be produced during both the light and dark periods. It can be inferred that the photoelectrons generated by CdS acted as the electron donors for the reduction of CO_2 to CH_4 by the biohybrid. Theoretically, no electrons can be generated under dark conditions, while CH_4 was still generated at these stages. Moreover, the CH_4 generation rate during the light period was higher than during the dark period counterpart. It was deduced that a part of the generated electrons was stored in the biohybrid during the light period, and these stored electrons can be released and used by the *M. barkeri* to reduce CO_2 to CH_4 under dark conditions. Moreover, the stored reductive intermediates (e.g., NADH, NADPH, ferredoxin, acetyl-CoA) during the light period might also be used by the biohybrid for CO_2 reduction into CH_4 [66].

The efficiency of photoelectron-hole separation in the *M. barkeri*-CdS biohybrid was determined by the photocurrent transient analysis (Fig. 3b). The *M. barkeri* exhibited a minimal and consistent linear photocurrent signal (14.9 $\mu A/cm^2$), reflecting bioelectric feedback from irradiation [67]. In contrast, CdS displayed a marginal increase in current density over time, indicating limited photocatalytic activity due to poor charge carrier separation [68]. Conversely, the *M. barkeri*-CdS biohybrid showed pronounced current fluctuations during light–dark cycles, achieving a significantly high current density (230 $\mu A/cm^2$) under light conditions. This enhancement is attributed to the superior photon absorption of CdS and a lower Fermi level, facilitating charge transfer across the interface. This stable current density suggests a more effective separation of electron–hole pairs, credited to the utilization of outer membrane-bound electron acceptors of the biohybrid [69]. Overall, the biohybrid has an outstanding performance on photoelectron generation as well as hole separation, which facilitates the CH_4 production by the *M. barkeri*-CdS biohybrid.

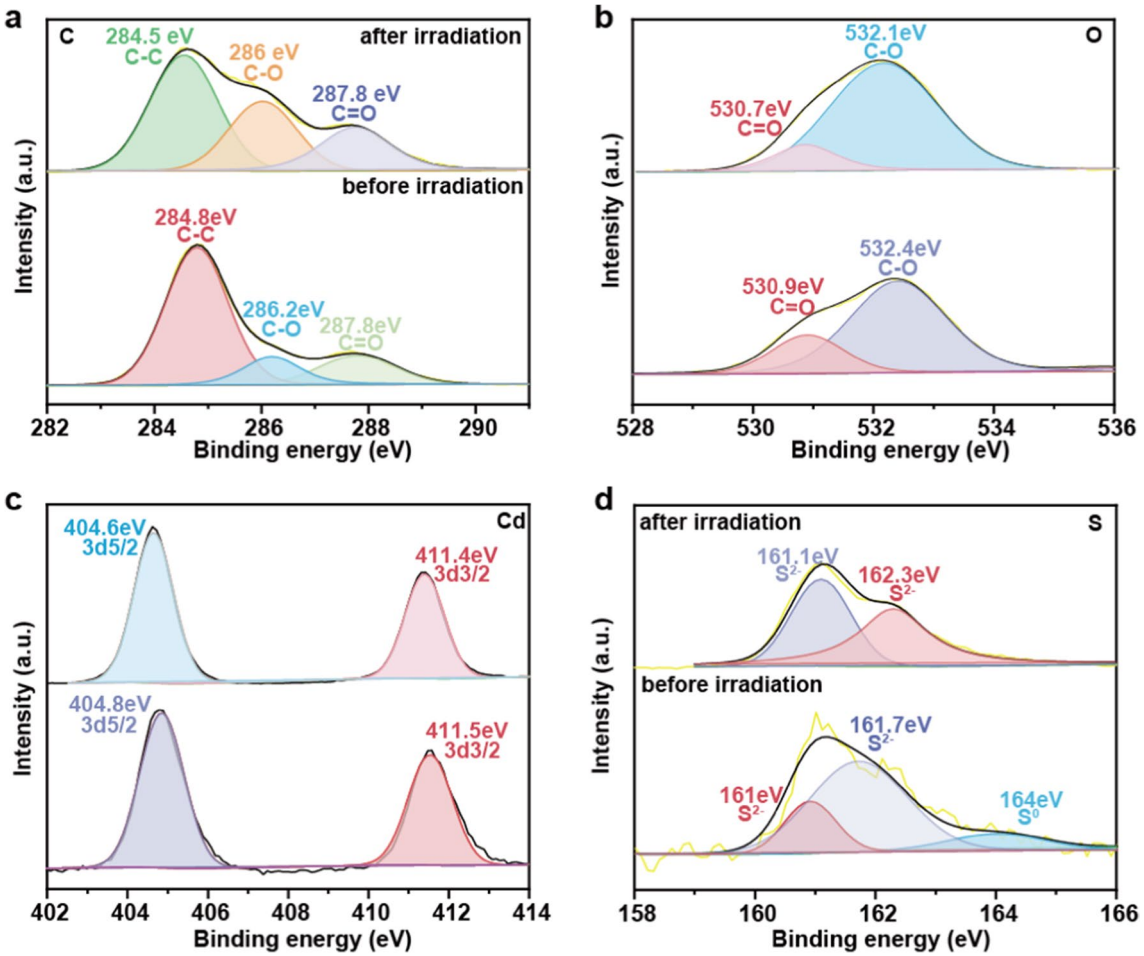

Fig. 4 (**A**) C 1s, (**B**) O 1s, (**C**) Cd 3d, and (**D**) S 2p XPS spectra of the biohybrid before and after irradiation

The photoelectrochemical characteristics of the *M. barkeri*-CdS biohybrid were further analyzed by EIS. In EIS Nyquist plots, a smaller semicircle radius indicates improved charge carrier transport [70]. In both dark and light conditions, the *M. barkeri*-CdS biohybrid exhibited a significantly small semicircle diameter compared to pure CdS and *M. barkeri* alone (Fig. 3c, Supplementary Fig. S3), suggesting a reduced electron transfer resistance and increased photocurrent density within the biohybrid. Furthermore, a decrease in impedance under light compared to dark conditions (Fig. 3d) indicated enhanced photoelectron production and conductance. UV–vis spectroscopy (Fig. 3e) showed the bandgap (Eg) of CdS reached 2.70 eV, likely due to quantum size effects [71]. The biohybrid displayed a wavelength of absorption edge (λg) at 470 nm and an Eg of 2.63 eV, confirming successful CdS doping on *M. barkeri* and extending the Eg of *M. barkeri* and λg of CdS. Importantly, the λg of *M. barkeri*-CdS (0.05 wt% Cys) exhibited a significant red-shift compared to *M. barkeri*-CdS (0.06 wt% Cys), indicating increased photocatalytic activity. The optimal Cys concentration led to a narrowed bandgap, optimizing visible light absorption without introducing localized states between the valence bands and conduction bands [72], which led to a higher CH_4 production.

The impact of light exposure on the chemical properties of the biohybrid was assessed by FT-IR (Fig. 3f). No obvious change in the peak positions of the biohybrid was observed, indicating no significant alterations for functional groups of the biohybrid before and after light exposure. This stability showed the robust structural integrity of this biohybrid under light exposure. Notably, a peak corresponding to the hydroxyl group (1028 cm^{-1}) was present in the biohybrid under the light condition. It was inferred that the photogenerated electrons interacted with the hydroxyl group, which facilitated electron transfer and inhibited electron–hole recombination in the biohybrid. Besides, *M. barkeri* is hydrophilic due to abundant electron-rich hydroxyl groups, contributing to the interaction with the CdS via hydrogen bond and electrostatic interactions. Under light conditions, CdS was capable of generating electrons

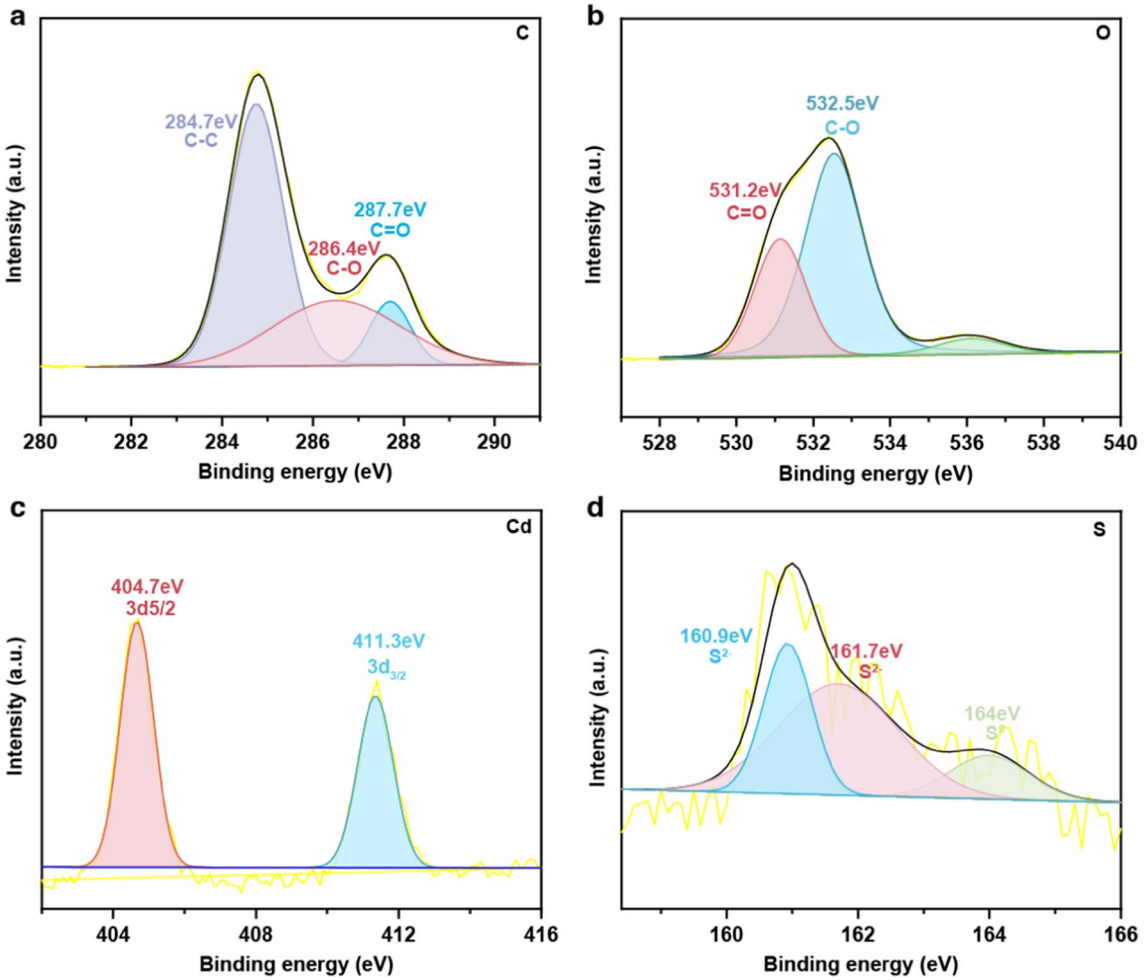

Fig. 5 (**A**) C 1s, (**B**) O 1s, (**C**) Cd 3d, and (**D**) S 2p XPS spectra of the biohybrid under dark condition

and holes, with the hydroxyl anion/radical redox couple efficiently transferring holes from the CdS to the scavenger. The hydroxyl group transfers from CdS to hydroxyl oxygen by accepting electrons, potentially enhancing the photocatalytic efficiency of the photocatalyst during the reaction.

XPS analysis was used to examine the valence changes of elements within the biohybrid before and after light exposure, providing insights into the electron transfer mechanism involved in CO_2 reduction to CH_4 by the biohybrid. The XPS spectrum identified C, O, S, and Cd as the main elements (Supplementary Fig. S2), with C, O, and Cd in the biohybrid maintaining stable valence states throughout the reaction (Fig. 4a–c). Notable changes were observed in the S 2p spectra before and after light exposure (Fig. 4d). It was proposed that the S can act as an effective electron transfer hub in biohybrid catalysts through valence state adjustments [73]. Initially, the S 2p spectrum peaked at 161 eV and 161.7 eV for S^{2-} and 164 eV for S^0. After light exposure, the peak location shifted, revealing predominant peaks for S^{2-} at 161.1 eV and 162.3 eV, while the peak for S^0 decreased. This indicates the dynamic electron interactions under light conditions. Therefore, the generated photoelectrons under light conditions were mainly used to convert CO_2 to CH_4 by the *M. barkeri*-CdS hybrid.

The valence state of the elements was also determined to disclose the electron transfer during CH_4 production by the biohybrid under dark conditions. The biohybrid was predominantly composed of C, O, Cd, and S (Fig. 5a–c). The changes in S valence were detected in biohybrid (Fig. 5d). The peaks at 164 eV corresponded to S^0, whereas those at 161.7 eV and 160.9 eV corresponded to S^{2-} [69]. Both S^{2-} and S^0 were detected in the biohybrid, with an increased intensity of S^0 after the reaction. It was inferred that S^{2-} was oxidized to S^0, providing electrons for the reduction of CO_2 to CH_4 by *M. barkeri* under dark conditions.

4 Conclusion

The *M. barkeri*-CdS biohybrid was successfully developed to enhance CO_2 reduction for CH_4 production under illuminated conditions. Optimal performance was achieved with a $CdCl_2$ dosage of 0.75 mM, pH of 8.36, $NaHCO_3$ concentration of 10 mM, and Cys concentration of 0.05 wt%. The biohybrid was demonstrated to be efficient in photoelectron generation, leading to a current with reduced impedance under light conditions. Photoelectrons generated under light conditions primarily drive the conversion of CO_2 to CH_4 by the *M. barkeri*-CdS biohybrid, whereas S^{2-} serves as the potential electron donor under dark conditions.

Author contributions Ziyu Wang: data curation, formal analysis, methodology, writing-original draft, writing-review & editing.
Mingyu Gou: data curation, visualization, methodology, formal analysis, writing-original draft, writing-review & editing.
Qiyuan Zheng: data curation, formal analysis.
Haiyu Xu: Methodology, writing-review & editing.
Saad Melhi: formal analysis, methodology, review & editing,
Zeinhom M. El-Bahy: formal analysis, methodology, review & editing.
Eman Ramadan Elsharkawy: formal analysis, methodology, review & editing.
Yan Dang: Conceptualization, methodology, writing-review & editing.
Bin Qiu: Conceptualization, project administration, investigation, methodology, writing-original draft, writing-review & editing.

Funding This work is sponsored by the Beijing Nova Program (20220484080). The authors extend their appreciation to the Deanship of Scientific Research at Northern Border University, Arar, KSA, for funding this research (NBU-FPEJ-2024–249-04).

Data availability The datasets generated from the current study will be provided upon reasonable request.

Declarations

Competing interests The authors declare no competing interests.

References

1. Chen X, Liu W, Zhao Y, He H, Ma J, Cui Z, Yuan X (2023) Optimization of semi-continuous dry anaerobic digestion process and biogas yield of dry yellow corn straw: based on "gradient anaerobic digestion reactor." Biores Technol 389:129804. https://doi.org/10.1016/j.biortech.2023.129804
2. Wang Z, He H, Yan J, Xu Z, Yang G, Wang H, Zhao Y, Cui Z, Yuan X (2024) Influence of temperature fluctuations on anaerobic digestion: optimum performance is achieved at 45 °C. Chem Eng J 492:152331. https://doi.org/10.1016/j.cej.2024.152331
3. Lu J, Yang Y, Zhing Y, Hu Q, Qiu B (2022) The study on activated carbon, magnetite, polyaniline and polypyrrole development of methane production improvement from wastewater treatment. ES Food Agrofor 10:30–38. https://doi.org/10.30919/esfaf802
4. Noori MT, Vu MT, Ali RB, Min B (2020) Recent advances in cathode materials and configurations for upgrading methane in bioelectrochemical systems integrated with anaerobic digestion. Chem Eng J 392:18. https://doi.org/10.1016/j.cej.2019.123689
5. Aghel B, Behaein S, Alobaid F (2022) CO_2 capture from biogas by biomass-based adsorbents: a review. Fuel 328:18. https://doi.org/10.1016/j.fuel.2022.125276
6. Wu L, Wei W, Song L, Wozniak-Karczewska M, Chrzanowski L, Ni BJ (2021) Upgrading biogas produced in anaerobic digestion: biological removal and bioconversion of CO_2 in biogas. Renew Sustain Energy Rev 150:22. https://doi.org/10.1016/j.rser.2021.111448
7. AbdulRasheed T, Afotey B, Ankudey EG, Anang DA (2023) Synthesis and characterization of novel calcium oxide/calcium ferrite, $CaO/CaFe_2O_4$ composite nanocatalyst for biodiesel production. ES Mater Manuf 22:922. https://doi.org/10.30919/esmm922
8. Das S, Goswami T, Ghosh A, Bhat M, Hait M, Jalgham RTT, Vidya L, Das R, Goswami J, Roymahapatra G (2024) Biodiesel from algal biomass: renewable, and environment-friendly solutions to global energy needs and its current status. ES Gen https://doi.org/10.30919/esg1133

9. Jamradloedluk J, Trisupakitti S (2023) Two-step biodiesel production from black acid oil waste using calcium oxide from charcoal ash as a catalyst. Eng Sci 28:1053. https://doi.org/10.30919/es1053
10. Roymahapatra G, Pradhan S, Sato S, Nakane D, Hait M, Bhattacharyya S, Saha R, Akitsu T (2023) Computational study on docking of laccase and cyanide-bridged Ag-Cu complex for designing the improved biofuel cell cathode. ES Energy Environ 21:957. https://doi.org/10.30919/esee957
11. Batlle-Vilanova P, Rovira-Alsina L, Puig S, Balaguer MD, Icaran P, Monsalvo VM, Rogalla F, Colprim J (2019) Biogas upgrading, CO_2 valorisation and economic revaluation of bioelectrochemical systems through anodic chlorine production in the framework of wastewater treatment plants. Sci Total Environ 690:352–360. https://doi.org/10.1016/j.scitotenv.2019.06.361
12. Fu S, Angelidaki I, Zhang Y (2021) *In situ* biogas upgrading by CO_2-to-CH_4 bioconversion. Trends Biotechnol 39:336–347. https://doi.org/10.1016/j.tibtech.2020.08.006
13. Iniyan S, Ren J, Deshmukh S, Rajeswaran K, Jegan G, Hou H, Suryanarayanan V, Murugadoss V, Kathiresan M, Xu B, Guo Z (2023) An overview of metal-organic framework based electrocatalysts: design and synthesis for electrochemical hydrogen evolution, oxygen evolution, and carbon dioxide reduction reactions. Chem Rec 23:e2023003. https://doi.org/10.1002/tcr.202300317
14. Shi J, Wang A, An Y, Chen S, Bi C, Qu L, Shi C, Kang F, Sun C, Huang Z, Qi H, Hu J (2024) Core@shell-structured catalysts based on Mg-O-Cu bond for highly selective photoreduction of carbon dioxide to methane. Adv Compos Hybrid Mater 7:2. https://doi.org/10.1007/s42114-023-00801-6
15. Hamukwaya SL, Zhao Z, Hao H, Abo-Dief HM, Abualnaja KM, Alanazi AK, Mashingaidze MM, El-Bahy SM, Huang M, Guo Z (2022) Enhanced photocatalytic performance for hydrogen production and carbon dioxide reduction by a mesoporous single-crystal-like TiO_2 composite catalyst. Adv Compos Hybrid Mater 5:2620–2630. https://doi.org/10.1007/s42114-022-00545-9
16. Brunetti A, Barbieri G (2022) Multi-step membrane process for biogas upgrading. J Membr Sci 652:10. https://doi.org/10.1016/j.memsci.2022.120454
17. Pellegrini LA, De Guido G, Langé S (2018) Biogas to liquefied biomethane via cryogenic upgrading technologies. Renew Energy 124:75–83. https://doi.org/10.1016/j.renene.2017.08.007
18. Vilardi G, Bassano C, Deiana P, Verdone N (2020) Exergy and energy analysis of biogas upgrading by pressure swing adsorption: dynamic analysis of the process. Energy Convers Manag 226:14. https://doi.org/10.1016/j.enconman.2020.113482
19. Wang H, Ma C, Yang Z, Lu X, Ji X (2020) Improving high-pressure water scrubbing through process integration and solvent selection for biogas upgrading. Appl Energy 276:11. https://doi.org/10.1016/j.apenergy.2020.115462
20. Yang H, Wang X, Liu J, Liu W, Gong Y, Sun Y (2022) Amine-impregnated polymeric resin with high CO_2 adsorption capacity for biogas upgrading. Chem Eng J 430:8. https://doi.org/10.1016/j.cej.2021.132899
21. Fu X, Li J, Pan X, Huang L, Li C, Cui S, Liu H, Tan Z, Li W (2020) A single microbial electrochemical system for CO_2 reduction and simultaneous biogas purification, upgrading and sulfur recovery. Biores Technol 297:4. https://doi.org/10.1016/j.biortech.2019.122448
22. Wang S, Han X, Zhang Y, Tian N, Ma T, Huang H (2020) Inside-and-out semiconductor engineering for CO_2 photoreduction: from recent advances to new trends. Small Structs 2:49. https://doi.org/10.1002/sstr.202000061
23. Lee C-Y, Zou J, Bullock J, Wallace GG (2019) Emerging approach in semiconductor photocatalysis: towards 3D architectures for efficient solar fuels generation in semi-artificial photosynthetic systems. J Photochem Photobiol C 39:142–160. https://doi.org/10.1016/j.jphotochemrev.2019.04.002
24. Sahoo PC, Pant D, Kumar M, Puri SK, Ramakumar SSV (2020) Material-microbe interfaces for solar-driven CO_2 bioelectrosynthesis. Trends Biotechnol 38:1245–1261. https://doi.org/10.1016/j.tibtech.2020.03.008
25. Cestellos-Blanco S, Zhang H, Kim JM, Shen Y, Yang P (2020) Photosynthetic semiconductor biohybrids for solar-driven biocatalysis. Nat Catal 3:245–255. https://doi.org/10.1038/s41929-020-0428-y
26. Wang R, Wang Y, Mao S, Hao X, Duan X, Wen Y (2021) Different morphology MoS_2 over the g-C_3N_4 as a boosted photo-catalyst for pollutant removal under visible-light. J Inorg Organomet Polym Mater 31:32–42. https://doi.org/10.1007/s10904-020-01626-2
27. Chamanehpour E, Sayadi MH, Hajiani M (2022) A hierarchical graphitic carbon nitride supported by metal–organic framework and copper nanocomposite as a novel bifunctional catalyst with long-term stability for enhanced carbon dioxide photoreduction under solar light irradiation. Adv Compos Hybrid Mater 5:2461–2477. https://doi.org/10.1007/s42114-022-00459-6
28. Hu L, Yang J, Xia Q, Zhang J, Zhao H, Lu Y (2024) Chemico-biological conversion of carbon dioxide. J Energy Chem 89:371–387. https://doi.org/10.1016/j.jechem.2023.10.058
29. Li L, Xu Z, Huang X (2021) Whole-cell-based photosynthetic biohybrid systems for energy and environmental applications. ChemPlusChem 86:1021–1036. https://doi.org/10.1002/cplu.202100171
30. Ye J, Yu J, Zhang Y, Chen M, Liu X, Zhou S, He Z (2019) Light-driven carbon dioxide reduction to methane by *Methanosarcina barkeri*-CdS biohybrid. Appl Catal B-Environ 257:8. https://doi.org/10.1016/j.apcatb.2019.117916
31. Ye J, Ren G, Kang L, Zhang Y, Liu X, Zhou S, He Z (2020) Efficient photoelectron capture by Ni decoration in *Methanosarcina barkeri*-CdS biohybrids for enhanced photocatalytic CO_2-to-CH_4 conversion. iScience 23:101287. https://doi.org/10.1016/j.isci.2020.101287
32. Ye J, Wang C, Gao C, Fu T, Yang C, Ren G, Lu J, Zhou S, Xiong Y (2022) Solar-driven methanogenesis with ultrahigh selectivity by turning down H_2 production at biotic-abiotic interface. Nat Commun 13:6612. https://doi.org/10.1038/s41467-022-34423-1
33. Hu A, Ye J, Ren G, Qi Y, Chen Y, Zhou S (2022) Metal-free semiconductor-based bio-nano hybrids for sustainable CO_2-to-CH_4 conversion with high quantum yield. Angew Chem-Int Ed 61:6. https://doi.org/10.1002/anie.202206508
34. Ye J, Chen Y, Gao C, Wang C, Hu A, Dong G, Chen Z, Zhou S, Xiong Y (2022) Sustainable conversion of microplastics to methane with ultrahigh selectivity by a biotic-abiotic hybrid photocatalytic system. Angew Chem-Int Ed 61:e202213244. https://doi.org/10.1002/anie.202213244
35. Chen M, Fang Z, Xu L, Zhou D, Yang X, Zhu H, Yong Y (2021) Enhancement of photo-driven biomethanation under visible light by nano-engineering of *Rhodopseudomonas palustris*. Bioresources Bioprocess 8:9. https://doi.org/10.1186/s40643-021-00383-5
36. Zhang W, Chen B, Li A, Zhang L, Li R, Yang T, Xing W (2019) Mechanism of process imbalance of long-term anaerobic digestion of food waste and role of trace elements in maintaining anaerobic process stability. Biores Technol 275:172–182. https://doi.org/10.1016/j.biortech.2018.12.052
37. Zhao Z, Wang J, Li Y, Zhu T, Yu Q, Wang T, Liang S, Zhang Y (2020) Why do DIETers like drinking: metagenomic analysis for methane and energy metabolism during anaerobic digestion with ethanol. Water Res 171:14. https://doi.org/10.1016/j.watres.2019.115425
38. Cheng L, Xiang Q, Liao Y, Zhang H (2018) CdS-based photocatalysts. Energy Environ Sci 11:1362–1391. https://doi.org/10.1039/c7ee03640j

39. Sun Q, Wang N, Yu J, Yu J (2018) A hollow porous CdS photocatalyst. Adv Mater 30:1804368. https://doi.org/10.1002/adma.201804368
40. Li J, Li Y, Qi M, Lin Q, Tang Z, Xu Y (2020) Selective organic transformations over cadmium sulfide-based photocatalysts. ACS Catal 10:6262–6280. https://doi.org/10.1021/acscatal.0c01567
41. Lin C, Zhang Y, Zhang S, Wang XX, Yang J, Li J, Lu X, Liu B, School Of Chemistry And Chemical Engineering X S Y U, School Of Materials Science Engineering Shan Dong University S J C (2023) Facile fabrication of a novel g-C_3N_4/CdS composites catalysts with enhanced photocatalytic performances. ES Energy Environ 20:860. https://doi.org/10.30919/esee8c
42 Jasmine J, Ponvel KM (2023) Synthesis of Ag_2CdS_2/carbon nanocomposites for effective solar-driven dye photodegradation and electrochemical application. ES Energy Environ 20:898. https://doi.org/10.30919/esee898
43. Liu G, Gao F, Zhang H, Wang L, Gao C, Xiong Y (2021) Biosynthetic CdS-*Thiobacillus thioparus* hybrid for solar-driven carbon dioxide fixation. Nano Res 16:4531–4538. https://doi.org/10.1007/s12274-021-3883-0
44. Ouyang L, Huang W, Huang M, Qiu B (2022) Polyaniline improves granulation and stability of aerobic granular sludge. Adv Compos Hybrid Mater 5:1126–1136. https://doi.org/10.1007/s42114-022-00450-1
45. Lu H, Zhao B, Pan R, Yao J, Qiu J, Luo L, Liu Y (2014) Safe and facile hydrogenation of commercial degussa P25 at room temperature with enhanced photocatalytic activity. RSC Adv 4:1128–1132. https://doi.org/10.1039/c3ra44493g
46. Zhang K, Liu X, Bi J, BaQais A, Xu BB, Amin MA, Hou Y, Liu X, Li H, Algadi H, Xu J, Guo Z (2023) Bimetallic NiCe/Lay catalysts facilitated co-pyrolysis of oleic acid and methanol for efficiently preparing anaerobic hydrocarbon fuels. New J Chem 47:18272–18284. https://doi.org/10.1039/d3nj01359f
47. Wang Y, Lu H, Wang Y, Qiu J, Wen J, Zhou K, Chen L, Song G, Yao J (2016) Facile synthesis of TaO*x*N*y* photocatalysts with enhanced visible photocatalytic activity. RSC Adv 6:1860–1864. https://doi.org/10.1039/c5ra23087j
48. Ka F, Saidi I, Ben Jannet H, Khairy M, Abdulkhair BY, Al-Ghamdi YO, Abdelhamid HN (2022) Chitosan-CdS quantum dots biohybrid for highly selective interaction with copper(II) ions. ACS Omega 7:21014–21024. https://doi.org/10.1021/acsomega.2c01793
49. Kim J, Cestellos-Blanco S, Shen YX, Cai R, Yang P (2022) Enhancing biohybrid CO_2 to multicarbon reduction via adapted whole-cell catalysts. Nano Lett 22:5503–5509. https://doi.org/10.1021/acs.nanolett.2c01576
50. Huang Y, Cai B, Dong H, Li H, Yuan J, Xu H, Wu H, Xu Z, Sun D, Dang Y, Holmes DE (2022) Enhancing anaerobic digestion of food waste with granular activated carbon immobilized with riboflavin. Sci Total Environ 851:158172. https://doi.org/10.1016/j.scitotenv.2022.158172
51. Kumar V, Singh N, Jana S, Rout SK, Dey RK, Singh GP (2021) Surface polar charge induced Ni loaded CdS heterostructure nanorod for efficient photo-catalytic hydrogen evolution. Int J Hydrogen Energy 46:16373–16386. https://doi.org/10.1016/j.ijhydene.2020.06.176
52. Bai L, Li S, Ding Z, Wang X (2020) Wet chemical synthesis of CdS/ZnO nanoparticle/nanorod hetero-structure for enhanced visible light disposal of Cr(VI) and methylene blue. Colloid Surface A. https://doi.org/10.1016/j.colsurfa.2020.125489
53. Jiang Z, Wang B, Yu J, Wang J, An T, Zhao H, Li H, Yuan S, Wong PK (2018) $AgInS_2/In_2S_3$ heterostructure sensitization of *Escherichia coli* for sustainable hydrogen production. Nano Energy 46:234–240. https://doi.org/10.1016/j.nanoen.2018.02.001
54. Yuan G, Zhao X, Liang Y, Peng L, Dong H, Xiao Y, Hu C, Hu H, Liu Y, Zheng M (2019) Small nitrogen-doped carbon dots as efficient nanoenhancer for boosting the electrochemical performance of three-dimensional graphene. J Colloid Interface Sci 536:628–637. https://doi.org/10.1016/j.jcis.2018.10.096
55. Wang J, Li X, Yan J, Yang Y (2022) Effects of heavy metal ions on microbial reductive dechlorination of 1, 2-dichloroethane and tetrachloroethene. Front Mar Sci 9:11. https://doi.org/10.3389/fmars.2022.881950
56. Hu A, Fu T, Ren G, Zhuang M, Yuan W, Zhong S, Zhou S (2022) Sustained biotic-abiotic hybrids methanogenesis enabled using metal-free black phosphorus/carbon nitride. Front Microbiol 13:10. https://doi.org/10.3389/fmicb.2022.957066
57. Wang J, Fu R, Wen S, Ning P, Helal MH, Salem MA, Xu BB, El-Bahy ZM, Huang M, Guo Z, Huang L, Wang Q (2022) Progress and current challenges for CO_2 capture materials from ambient air. Adv Compos Hybrid Mater 5:2721–2759. https://doi.org/10.1007/s42114-022-00567-3
58. He P, Duan H, Han W, Liu Y, Shao L, Lü F (2019) Responses of *Methanosarcina barkeri* to acetate stress. Biotechnol Biofuels 12:14. https://doi.org/10.1186/s13068-019-1630-5
59. Duan H, He P, Zhang H, Shao L, Lü F (2022) Metabolic regulation of mesophilic *Methanosarcina barkeri* to ammonium inhibition. Environ Sci Technol 56:8897–8907. https://doi.org/10.1021/acs.est.2c01212
60. Lee E, Bittencourt P, Casimir L, Jimenez E, Wang M, Zhang Q, Ergas SJ (2019) Biogas production from high solids anaerobic co-digestion of food waste, yard waste and waste activated sludge. Waste Manag 95:432–439. https://doi.org/10.1016/j.wasman.2019.06.033
61. Lee J, Kim E, Hwang S (2021) Effects of inhibitions by sodium ion and ammonia and different inocula on acetate-utilizing methanogenesis: methanogenic activity and succession of methanogens. Biores Technol 334:125202. https://doi.org/10.1016/j.biortech.2021.125202
62. Valença RB, dos Santos LA, Firmo AL, da Silva LC, de Lucena TV, Santos AF, Jucá JF (2021) Influence of sodium bicarbonate ($NaHCO_3$) on the methane generation potential of organic food waste. J Clean Prod 317:8. https://doi.org/10.1016/j.jclepro.2021.128390
63. Chen M, Zhou X, Yu Y, Liu X, Zeng R, Zhou S, He Z (2019) Light-driven nitrous oxide production via autotrophic denitrification by self-photosensitized *Thiobacillus denitrificans*. Environ Int 127:353–360. https://doi.org/10.1016/j.envint.2019.03.045
64. Wang B, Xiao K, Jiang Z, Wang J, Yu J, Wong P (2019) Biohybrid photoheterotrophic metabolism for significant enhancement of biological nitrogen fixation in pure microbial cultures. Energy Environ Sci 12:2185–2191. https://doi.org/10.1039/c9ee00705a
65 Zhang K, Li R, Chen J, Chai L, Lin Z, Zou L, Shi Y (2024) Biohybrids of twinning $Cd_{0.8}Zn_{0.2}S$ nanoparticles and *Sporomusa ovata* for efficient solar-driven reduction of CO_2 to acetate. Appl Catal B: Environ 342:11. https://doi.org/10.1016/j.apcatb.2023.123375
66. Ye J, Chen Y, Gao C, Wang C, Hu A, Dong G, Chen Z, Zhou S, Xiong Y (2022) Sustainable conversion of microplastics to methane with ultrahigh selectivity by a biotic-abiotic hybrid photocatalytic system. Angew Chem-Int Ed 61:8. https://doi.org/10.1002/anie.202213244
67. Wu H, Feng X, Wang L, Chen C, Wu P, Li L, Xu J, Qi F, Zhang S, Huo F, Zhang W (2023) Solar energy for value-added chemical production by light- powered microbial factories. CCS Chem 10.31635. https://doi.org/10.31635/ccschem.023.202303011
68. Guo C, Tian K, Wang L, Liang F, Wang F, Chen D, Ning J, Zhong Y, Hu Y (2021) Approach of fermi level and electron-trap level in cadmium sulfide nanorods via molybdenum doping with enhanced carrier separation for boosted photocatalytic hydrogen production. J Colloid Interface Sci 583:661–671. https://doi.org/10.1016/j.jcis.2020.09.093

69. Yi X, Liu S, Luo M, Li Q, Wang Y (2022) An outer membrane photosensitized *Geobacter Sulfurreducens*-CdS biohybrid for redox transformation of Cr(VI) and tetracycline. J Hazard Mater 431:11. https://doi.org/10.1016/j.jhazmat.2022.128633
70. Kang F, Jiang X, Wang Y, Ren J, Xu B, Gao G, Huang Z, Guo Z (2023) Electron-rich biochar enhanced Z-scheme heterojunctioned bismuth tungstate/bismuth oxyiodide removing tetracycline. Inorg Chem Front 10:6045–6057. https://doi.org/10.1039/d3qi01283b
71. Zhang S, Li C, Ke C, Liu S, Yao Q, Huang W, Dang Z, Guo C (2023) Extracellular polymeric substances sustain photoreduction of Cr(VI) by *Shewanella oneidensis*-CdS biohybrid system. Water Res 243:120339. https://doi.org/10.1016/j.watres.2023.120339
72. Wang Y, Zhang Y, Lu H, Chen Y, Liu Z, Su S, Xue Y, Yao J, Zeng H (2018) Novel N-doped ZrO_2 with enhanced visible-light photocatalytic activity for hydrogen production and degradation of organic dyes. RSC Adv 8:6752–6758. https://doi.org/10.1039/c7ra12938f
73. Wang C, Yu J, Ren G, Hu A, Liu X, Chen Y, Ye J, Zhou S, He Z (2022) Self-replicating biophotoelectrochemistry system for sustainable CO methanation. Environ Sci Technol 56:4587–4596. https://doi.org/10.1021/acs.est.1c08340